Journal of Geophysical Research: Oceans

RESEARCH ARTICLE
10.1002/2017JC013364

Reconstruction of Snow on Arctic Sea Ice

E. Blanchard-Wrigglesworth[1], M. A. Webster[2], S. L. Farrell[3,4], and C. M. Bitz[1]

[1]Department of Atmospheric Sciences, University of Washington, Seattle, WA, USA, [2]NASA Goddard Space Flight Center, Greenbelt, MD, USA, [3]Earth System Science Interdisciplinary Center, University of Maryland, College Park, MD, USA, [4]NOAA Laboratory for Satellite Altimetry, NCWCP, College Park, MD, USA

Key Points:
- Sea ice motion and reanalysis snowfall can be used to reconstruct Arctic spring snow on sea ice at the large scale, local scale is low skill
- The eastern Arctic, particularly the Atlantic sector, shows deep snow cover even in regions of first-year ice
- Differences between reconstruction and the Warren snow climatology: use of latter may result in biased ice thickness satellite retrievals

Correspondence to:
E. Blanchard-Wrigglesworth,
ed@atmos.washington.edu

Citation:
Blanchard-Wrigglesworth, E., Webster, M. A., Farrell, S. L., & Bitz, C. M. (2018). Reconstruction of snow on Arctic Sea Ice. *Journal of Geophysical Research: Oceans*, *123*, 3588–3602. https://doi.org/10.1002/2017JC013364

Received 15 AUG 2017
Accepted 23 FEB 2018
Accepted article online 23 MAR 2018
Published online 20 MAY 2018

Abstract Snow on Arctic sea ice is a poorly observed variable that plays an important role in the Arctic climate system and impacts the remote sensing systems that monitor Arctic sea ice. We present and validate a reconstruction of Arctic snow depth based on observed sea ice motion and snowfall derived from reanalysis data. Overall, the reconstruction is in good agreement with direct measurements of snow depth from Operation IceBridge, slightly underestimating mean IceBridge snow depth. At the local scale (10 km), the reconstruction is more skilled than a weighted climatology over first year ice, but underestimates deeper snow over multi-year ice. Reconstructions of single buoy snow depths are unskilled, but the reconstruction shows skill in simulating the mean snow depth across all buoys. Spring snow depths show a low-to-high cross-Arctic gradient and tend to be greatest in the Atlantic sector of the eastern Arctic. The relationship between ice type (multiyear or first-year ice) and snow depth previously documented in the western Arctic is not evident in the eastern Arctic. Using ice type to weight snow depths for satellite ice thickness retrievals may not be justifiable in the eastern Arctic. Reconstructed snow depth across the Arctic shows significant interannual variability, suggesting that use of a fixed snow depth climatology may lead to biases in retrieved ice thickness and its variability. However, interannual variability in pan-Arctic mean snow depth is comparable or smaller than the uncertainty in both the reconstruction and IceBridge, highlighting the need for high accuracy snow depth products and reconstructions.

1. Introduction

Snow on sea ice plays an important role in the Arctic climate system and impacts the interpretation of data collected by the remote sensing systems used to monitor Arctic sea ice. Its presence in early summer delays the onset of ice melt while it has a higher albedo than bare sea ice or open ocean (Perovich et al., 2002). During the winter, it acts as an insulator and therefore reduces the heat loss from the ice/ocean to the atmosphere and slows down sea ice growth (e.g., Maykut & Untersteiner, 1971; Sturm et al., 2002a). Snow also impacts the formation of melt ponds (e.g., Petrich et al., 2012; Webster et al., 2015), which play a role in the energy budget of the Arctic and summer melt of the ice pack.

Much of the information used to monitor Arctic sea ice thickness derives from altimeters on remote sensing satellites that sample freeboard, the height of the snow/sea-ice interface above local sea level (e.g., Laxon et al., 2003). Sea ice thickness can be retrieved from the sampled freeboard, but values for snow depth and the density of ice, snow and sea water are needed in the calculation. Since these are not directly sampled or known in real time, climatological values are often used (e.g., Laxon et al., 2013). Uncertainty in the snow depth used in these calculations is the largest source of error in sea ice thickness (Giles et al., 2007).

The importance snow holds stands in stark contrast to our ability to monitor it, as direct observations of snow on sea ice have been sparse in space and time. The snow climatology of Warren et al. (1999) is widely used with satellite altimeter freeboard measurements to derive sea ice thickness since it offers needed monthly pan-Arctic maps of snow depth (e.g., Kwok & Cunningham, 2015; Laxon et al., 2013; Ricker et al., 2014; Tilling et al., 2015). Alternatively some investigators have made use of reanalysis snowfall and satellite derived sea-ice motion data in combination with ICESat freeboard measurements to retrieve ice thickness (e.g., Kurtz et al., 2011; Kwok & Cunningham, 2008), though we note that these studies did not validate their reconstructed snow-depth fields. The Warren et al. (1999) snow climatology is derived from observations collected at drifting Soviet stations on multiyear ice over the period 1954–1991. Due to their geographic

pattern of deployment and drift patterns large areas of the sea-ice cover were left unsampled, particularly north of Svalbard, Greenland, and the Canadian Arctic Archipelago. Since then the Arctic cryosphere has undergone significant changes, highlighted by a rapid decline in sea ice extent and thickness (Comiso et al., 2008; Kwok & Rothrock, 2009), a loss of multiyear sea ice (MYI) in favor of first-year sea ice (FYI) (Maslanik et al., 2011), and a reduction of snow depth in the western Arctic (Webster et al., 2014).

Direct snow depth observations are available from ice mass-balance buoys (IMBs) placed in drifting ice floes that generally sample over a period of 1–2 years (Richter-Menge et al., 2006), from in situ measurements collected at field survey sites at specific times and locations (e.g., Sturm et al., 2002b), from airborne snow radar sensors (e.g., Farrell et al., 2012) and from snow buoys deployed directly on ice floes (e.g., Itkin et al., 2017). The most extensive airborne survey is NASA's ongoing Operation IceBridge (OIB) mission, which since 2009 has flown yearly trans-oceanic surveys in the western Arctic of sea ice properties between mid-March and early May (Koenig et al., 2010).

Kurtz and Farrell (2011) and Blanchard-Wrigglesworth et al. (2015) analyzed IceBridge surveys and found spring snow depth distributions are significantly different over MYI and FYI, with mean depths of 31 cm and 16 cm respectively in 2009 (Kurtz & Farrell, 2011) and 32 cm and 20 cm respectively in 2011/2012 (Blanchard-Wrigglesworth et al., 2015). It has been proposed that the longer snow accumulation season over MYI together with peak precipitation in the fall are mainly responsible for the different snow depth distributions (Hezel et al., 2012), since in late summer and early fall most FYI has not yet formed and therefore FYI does not accumulate snow during this time, while MYI does. The observed spring snow depths are considered to represent snow accumulation since the previous summer, as snow generally completely melts every summer and over all ice types (e.g., Lindsay, 1998).

In this work, we present a reconstruction of snow depth over Arctic sea ice using snowfall data from atmospheric reanalysis products, satellite-derived ice motion data, and a Lagrangian ice tracking system. We compare this reconstruction to direct measurements of snow depth obtained from OIB and IMBs, and a snow depth climatology, we examine differences in snow depth between ice types across the Arctic, and we consider the utility of reanalysis products for use in deriving sea ice thickness from satellite altimeter data.

2. Data

The basis of our reconstruction is 12 hourly snowfall data from several reanalysis and precipitation products, focusing mainly on the ERA-Interim reanalysis (Dee et al., 2011). In reanalysis, snowfall (and precipitation in general) is a prognostic variable that is not assimilated and is constrained primarily through its relation to other observables. While evaluating Arctic precipitation in reanalysis is difficult due to the scarcity of direct observations and the fact that most precipitation in the Arctic falls as snow, which is notoriously difficult to measure accurately (Serreze et al., 2005), ERA-Interim is one of the higher fidelity reanalysis for Arctic precipitation (Lindsay et al., 2014). We use weekly-averaged sea ice velocities from the National Snow and Ice Data Center (NSIDC) Polar Pathfinder Daily 25 km resolution Equal Area Scalable Earth (EASE) grid product, version 3 (Tschudi et al., 2016), and weekly-averaged sea ice concentration from the NOAA-NSIDC Climate Data Record of Passive Microwave Sea Ice Concentration, version 2 (Meier et al., 2013). We also use the daily sea-ice type product of the EUMETSAT Ocean and Sea Ice Satellite Application Facility (OSI SAF, www.osi-saf.org) to delineate between first-year and multiyear sea ice. Ice classes are assigned from atmospherically corrected SSMIS brightness temperatures and ASCAT backscatter values and are provided on a polar stereographic 10 km grid (Breivik et al., 2012). For each year, we calculate the mean MYI/FYI boundary over the first 10 days of April. In grid cells where ice type is unclassified on a certain day, we use the median ice type over the remaining days to assign a MYI or FYI value to that grid cell.

To evaluate our snow depth reconstruction we use snow depth measurements from two sources: OIB and IMB. OIB operates a frequency modulated continuous-wave (FMCW) snow radar that has been flown on low-elevation flights over Arctic sea ice during early spring (mid March to late April) since 2009. Here we utilize OIB snow depth measurements derived using the wavelet methodology described in Newman et al. (2014). These techniques were applied to deconvolved OIB FMCW snow radar echograms provided in the IRSNO1B product distributed by the National Snow and Ice Data Center (Leuschen, 2010, updated 2017). The observations provide a record of snow depth across the western Arctic, at the end of winter, for 2009–2012 and 2014–2015, and have an uncertainty of ~6 cm (Newman et al., 2014). The wavelet methodology

adapts to changes in radar bandwidth and does not depend on a set of fixed thresholds or require tuning due to changing radar conditions, such as changes in transmitted power and receiver noise that vary both during, and between, different OIB flight campaigns. No data are available for 2013 due to the impact of side-lobes on the quality of the FMCW radar data (Yan et al., 2017) that could not be resolved through deconvolution techniques. To compare with our reconstruction, we apply an arithmetic mean to OIB data at an along-track resolution of 10 km.

IMB snow depths are taken from the Cold Regions and Research Engineering Laboratory IMBs (Perovich et al., 2017). The buoys are equipped with a downward-facing acoustic sounder that measures the position of the snow or sea ice surface with an accuracy of less than $\pm$ 1 cm. Upon deployment, the initial snow depth, if present, is measured so that changes in snow depth can be monitored throughout the lifetime of the buoy. Data were recorded at 4 hourly intervals and for the purpose of this analysis averaged to weekly values. Erroneous recordings can result from the buoy slipping in melting ice, the presence of large snow drifts, instrumental artifacts, and other issues. Erroneous values were removed when it was possible to objectively discern such issues using webcam imagery from co-located buoys and/or through thorough examination of the thermistor and meteorological data (see the SI for further details).

3. Methods

Our goal is to reconstruct snow depth from accumulated cold-season snowfall along sea-ice drift trajectories. To this end we use the Lagrangian Ice Tracking System (LITS) developed by DeRepentigny et al. (2016). The LITS uses weekly sea-ice motion fields to track parcels of ice in time and has an accuracy of $\sim$50 km after 6 months of tracking (see Figure 2 in DeRepentigny et al., 2016). At each time-step, a condition for the presence of sea-ice is imposed: if the value of sea ice concentration at the parcel's projected grid cell falls below 15%, the tracking stops and the trajectory is ended at the previous time-step. Our results are not overly sensitive to the 15% threshold (choosing 50% does not impact our findings, not shown), likely due to the rapid (from a weekly perspective) transition from open water to sea ice in the fall as the sea-ice edge moves southward. To produce early-spring Arctic maps of snow depth reconstructions, we create an initial regular grid with 75 km spacing between grid points and backtrack each grid point from the first week of April to the last week of the previous August. To compare our reconstruction methodology to the IMB buoy snow time series, we use the LITS to forward track the buoys' positions from their deployment dates in late summer/early fall through to the following spring (see Figure 5 for a display of buoy lifetimes). Once we have calculated a set of trajectories, we accumulate weekly averaged ERA-Interim snowfall S along the trajectories, as described in equation (1):

$$S(L,T) = \rho_T \sum_{t=1}^{T} s_{l,t}, \tag{1}$$

where S is snow depth at time T and location L, ρ_T is the density of snow at time T, $s_{l,t}$ is snowfall at time t and location l, calculated by the LITS. We use ρ_T here since snowfall in ERA-Interim is given in snow water equivalent (SWE) units and we wish to compare with observed snow depth values. However, values of ρ_T are not estimated either in ERA-Interim, OIB or IMBs, so we use the climatological monthly values provided by Warren et al. (1999).

4. Results

4.1. Spatial Reconstruction and Comparison With OIB

Figure 1 shows reconstructed April snow depths (S) from accumulated snowfall, OIB snow depths and the multiyear/first-year ice type boundary (where both are 50%) for years 2009–2015. The snowfall reconstruction shows that in most years there tends to be a gradient from thinner snow north of Alaska/East Siberia to deeper snow north of Svalbard. From visual inspection, it is apparent that in some years, there is a high degree of agreement between OIB snow depths and the reconstruction (e.g., 2011, 2012, 2015), yet less in other years (e.g., 2009, 2014). Interestingly, in the reconstruction there is no clear relationship between ice type and reconstructed snow depth either in space or time. Some years tend to have higher reconstructed snow depth over MYI relative to FYI (e.g., 2015), while others have almost the opposite (e.g., 2011). The

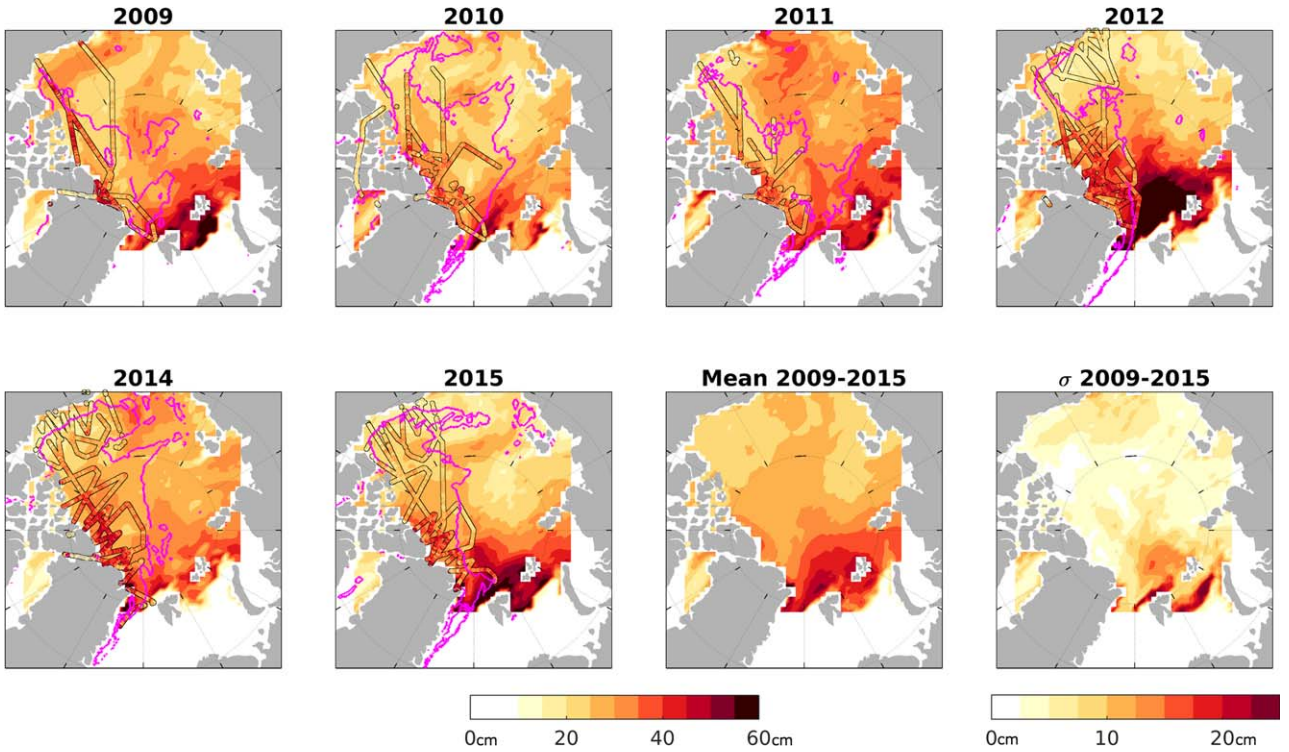

Figure 1. Reconstructed spring snow depth *S* and OIB snow depth in cm for 2009–2015. The magenta contours indicate the first-year/multiyear ice boundary. The bottom right plot shows the interannual standard deviation (σ) of reconstructed snow depth for 2009–2015.

Beaufort sea always tends to have a thin snow cover, irrespective of ice type present. Interannual variability of reconstructed snow depth is highest in the Atlantic sector, and to a lesser degree in the Chukchi sea.

To further assess the similarity between IceBridge and reconstructed snow depths, in Figure 2a we show histograms of OIB snow depth and the reconstructed snow depth along the OIB flight paths (in other words, snow depth values obtained from sampling the reconstruction fields in Figure 1 along the OIB flight paths) for each year over all ice types. Confirming visual inspection of Figure 1, there is good agreement in 2011, 2012, and 2015, while slightly less agreement in 2009, 2010, and 2014. Overall, the reconstruction snow depth tends to capture the thinner snow depths in the OIB distribution more accurately than the thicker snow depths (Figure 2g), and on average is slightly thinner than the OIB snow depth (2009–2015 mean of 27.9 cm in the reconstruction and 30.9 cm in OIB). In most years, the reconstructed snow depth also has a narrower distribution. This is not surprising, for the following reasons – firstly, the OIB averaging interval samples snow depths at higher resolution in space than the reconstruction (10 km versus 75 km). Given the high variability of snow depth at small spatial scales (e.g., Sturm et al., 2002b), a finer grid interval would capture more extreme depths and result in a broader OIB distribution even when compared to a perfect reconstruction (e.g., built from OIB data alone) but at a coarser resolution (e.g., on a 1 km-grid, the OIB snow depths have a 40% wider distribution than the 10 km-grid used here, not shown). Secondly, in the reconstruction we have used a constant monthly density ρ_T to compute snow depth from accumulated water equivalent snowfall. Spatial variations in density would result in a more variable distribution of the reconstruction snow depth. Finally, the reconstruction neglects any local scale mechanisms of redistribution (e.g., wind transport, snow loss to leads) that would lead to a wider distribution in snow depths in observations.

A high bias in the mean reconstructed snow depth might be expected since it neglects snow loss mechanisms (chiefly wind transport of snow into leads, sublimation, and divergence of the ice pack, see below). The fact that our reconstructed mean is slightly thinner than the OIB mean indicates that snow loss is either negligible, ERA-Interim is biased low (too little snowfall), the snow density used for the reconstruction is too high, OIB snow depths are biased high (Kwok et al., 2017), or a combination of all four factors.

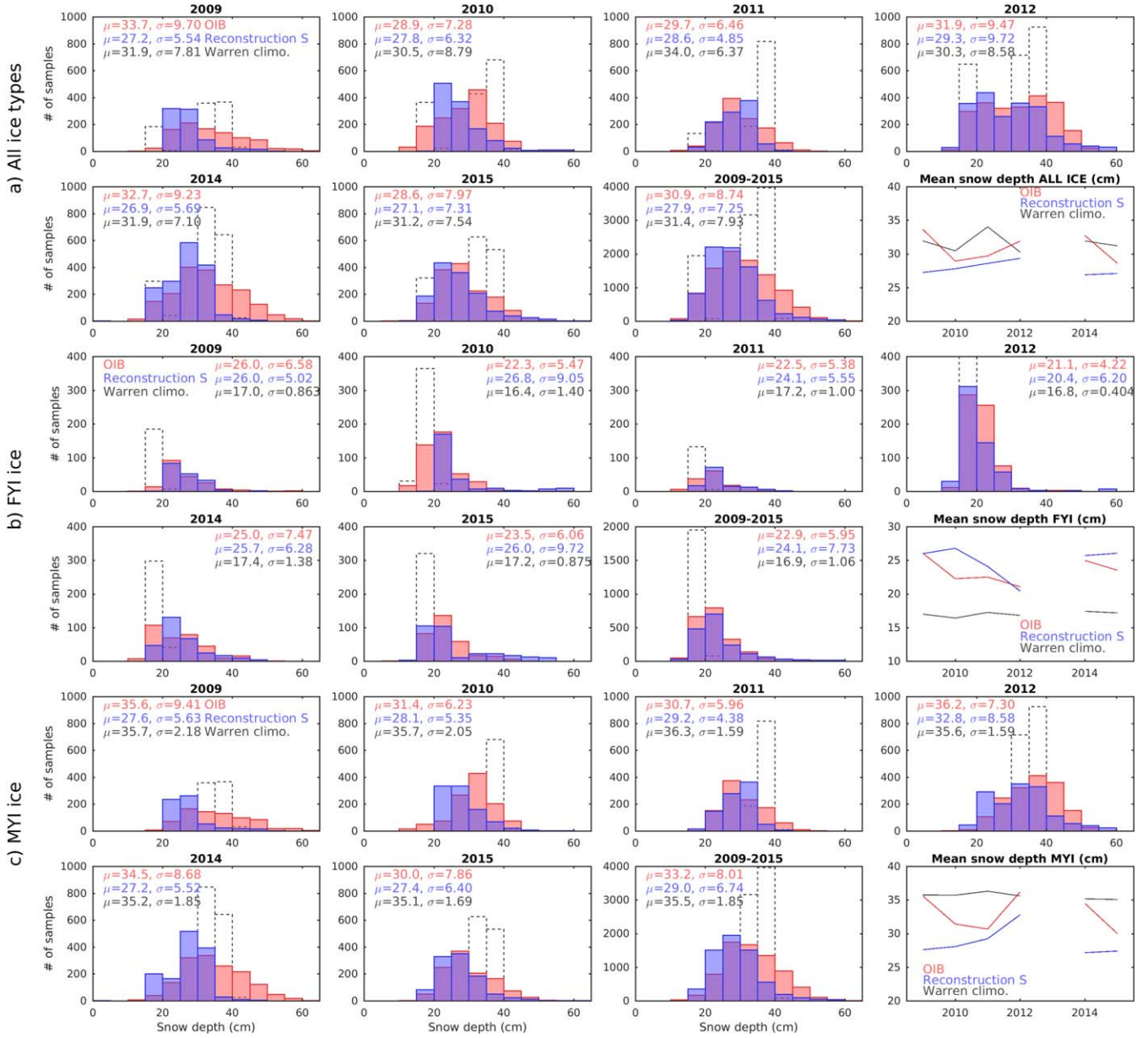

Figure 2. Histogram of snow depth from the OIB flights 2009–2015 (red), the reconstruction *S* (blue) and the weighted climatology (dashed black) sampled along OIB flightpaths and dates. The means and standard deviations across distributions are shown in the top of each plot. We show values over all ice types (top two rows), FYI (middle two rows), and MYI (bottom two rows).

In Figures 2b and 2c, we show the snow depth distributions for the reconstruction and OIB over FYI and MYI respectively. Over FYI, the reconstruction simulates OIB with high fidelity (2009–2015 mean of 24.1 cm in the reconstruction and 22.9 cm in OIB). Over MYI, the reconstruction is biased thin, generally not capturing the deeper snow depths in OIB (2009–2015 mean of 29.0 cm in the reconstruction and 33.2 cm in OIB).

4.2. Comparison With the Warren Snow Climatology

Satellite-derived estimates of sea ice thickness obtained from freeboard measurements often make use of snow depths from the Warren et al. (1999) monthly climatology. Recently, some investigators have weighted the climatological snow depths by ice type: for MYI, the climatological snow depth is used, while for FYI, climatological snow depth is reduced. For example, sea-ice thickness retrievals by Laxon et al. (2013) and Tilling et al. (2015) both used snow depths on FYI were half of the climatological value, while *Kwok and*

Cunningham (2015) investigated the consequences of weighting by 0.5 and 0.7. The justification for this ice-type dependent weighting originates from Kurtz and Farrell (2011) who found that snow depth over FYI was approximately half the snow depth over MYI in OIB measurements collected in March/April 2009. Although OIB measurements sample almost exclusively the western Arctic, weighting by a constant factor is commonly applied across the Arctic in satellite sea-ice thickness retrievals.

Figure 2 also shows the snow depth distributions over the OIB domain of the weighted Warren climatology (hereafter termed weighted climatology) in which snow depths on FYI are multiplied by 0.5. Overall, the mean snow depth values from the weighted climatology are in close agreement with OIB values (2009–2015 mean of 31.4 cm versus 30.9 cm for OIB), although the weighted climatology distribution shape is strongly biased as it is bimodal in every year. Considering snow over FYI (Figure 2b), the weighted climatology is too thin (2009–2015 mean of 16.9 cm versus 22.9 cm for OIB). Over MYI (Figure 2c), the weighted climatology is too deep (2009–2015 mean of 35.5 cm versus 33.2 cm for OIB). Over both ice types, the weighted climatology cannot capture the interannual variability seen in both OIB and the reconstruction, and its distribution is biased narrow.

To further investigate the skill of the reconstruction relative to the weighted climatology, we show scatter plots of the individual OIB data points with the reconstruction and weighted climatology in Figure 3. As suggested by Figure 1, the skill of the reconstruction (and weighted climatology) varies considerably from year to year. Overall, the reconstruction does not improve on the weighted climatology as characterized by correlation and RMSE metrics ($R_S = 0.49$, $R_{wclim} = 0.53$, $RMSE_S = 8.3$ cm, $R_{wclim} = 7.7$ cm). The main source of error of the reconstruction is the lower skill in capturing the deeper snowdepths in OIB.

Differentiating skill over each ice type, the reconstruction shows better skill than the weighted climatology over FYI (Figure 3b, $R_S = 0.58$, $R_{wclim} = 0.49$, $RMSE_S = 6.5$ cm, $R_{wclim} = 8.2$ cm). Over MYI (Figure 3c), the reconstruction underestimates the deeper OIB snow depths, and is similar in skill to the weighted climatology ($R_S = 0.39$, $R_{wclim} = 0.30$, $RMSE_S = 8.8$ cm, $R_{wclim} = 7.6$ cm).

In Figure 4 we show the difference in snow water equivalent (SWE) between our reconstruction (Figure 1) and the weighted climatology. For the weighted climatology, we average March and April as an estimate of early April. Figure 4 shows a large difference between our reconstruction and the weighted climatology. In the western Arctic (and mainly over MYI), the reconstruction tends to be 0–6 cm SWE less than the weighted climatology. This result is in broad agreement with previous work by Webster et al. (2014), who found a thinning of ~13 cm snow depth (equivalent to a ~4 cm SWE loss using a mean snow density of 320 kg/m^3) in the western Arctic between the time period represented in the Warren climatology and the period of OIB observations. In the eastern Arctic, in contrast, our reconstructed snow depths are generally 0–10 cm SWE greater than the weighted climatology (note that, since most ice in the eastern Arctic is FYI, the weighted climatology in this region is roughly half the original Warren climatology). The largest RMSE values (Figure 4) are found in the Atlantic sector of the Arctic, particularly in the Nansen Basin and Kara and Barents seas. We discuss the implications of these results for satellite-derived estimates of sea ice thickness below.

4.3. Comparison With IMBs

We now compare the snow depth reconstruction with observed snow depths from drifting IMBs. Figure 5 lists the timelines of buoys used and when quality-controlled snow data are available. Of the 19 IMBs analyzed, two buoys exhibited unusual drift patterns that were likely due to erroneous GPS readings. IMBs 2010E and 2010F remained static or shifted back and forth toward the Alaskan coast despite the observed ice drift from other buoy data in the same vicinity in 2010 (International Arctic Buoy Programme) and that modeled by LITS, which captures other buoy tracks accurately (Figure 6). Additionally, the sounder data for 2010F showed unusually flat-lined snow depths, suggesting that no significant accumulation or melting had occurred. Using O-buoy webcam imagery from the same location (http://obuoy.datatransport.org/monitor#buoy2/movie), we found that snowfall and blowing snow events had occurred and, in June, melt ponds had formed despite the 2010F sounder data showing little change in snow depth. IMB buoy 2013F recorded an uncharacteristically large accumulation event between 19 and 22 of October 2013, likely a result of a snow drift forming under the acoustic sounder, as 21 cm snowfall events within a 48 h period are unusual for the Beaufort Sea region.

Figure 7 shows the time series of IMB and reconstructed snow depths. Generally, there is a poor match between individual buoys and the reconstruction. Individual buoys can have much deeper snow depths

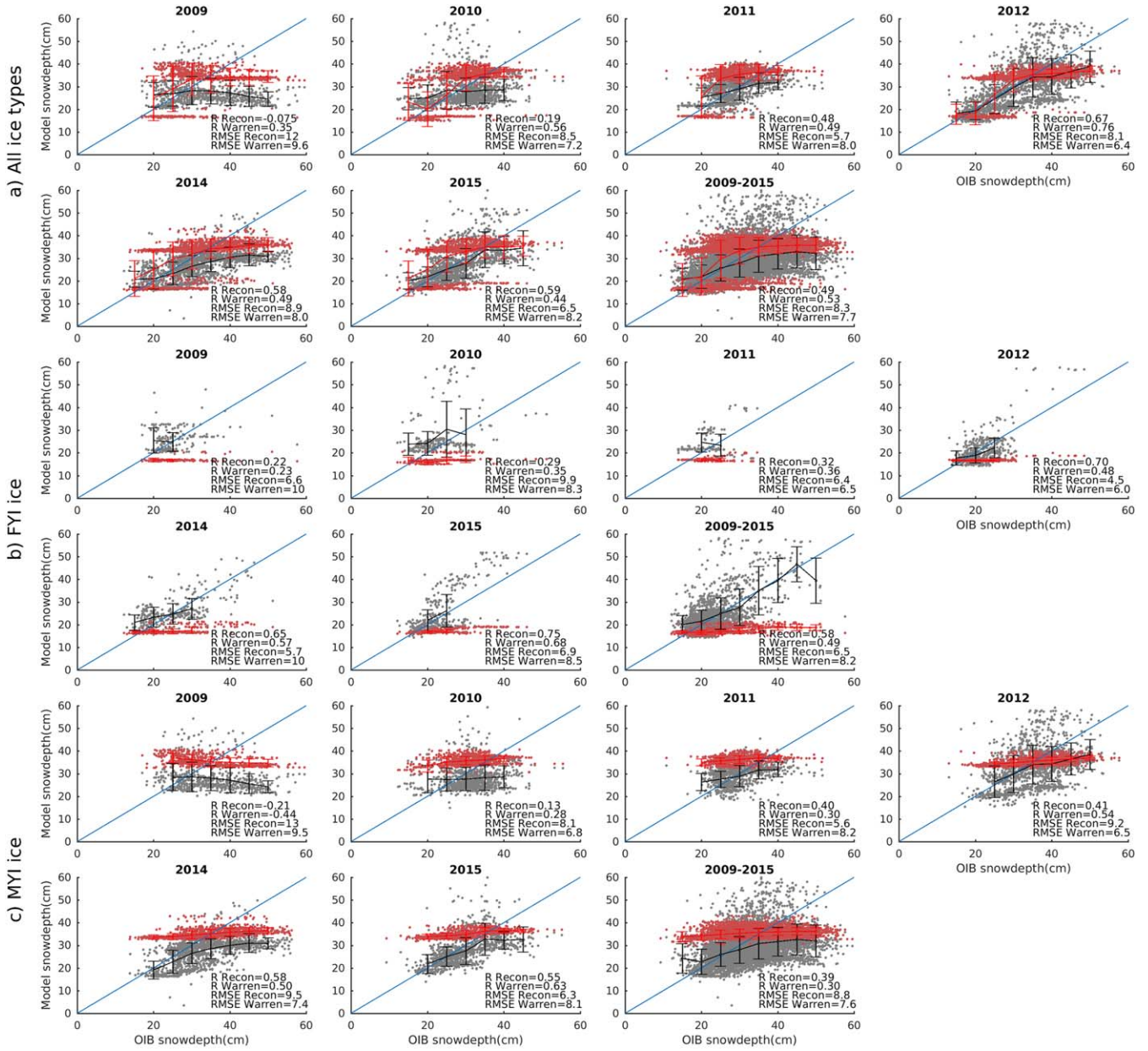

Figure 3. Scatterplots of snow depth from the OIB flights 2009–2015 and the snowfall reconstruction (black dots) and weighted climatology (red dots) along those same flightpaths. Correlation R and RMSE values are shown at plots' bottom right. We show values over all ice types (top two rows), FYI (middle two rows), and MYI (bottom two rows).

than the reconstruction (e.g., by 20–30 cm in 2013F) or thinner snow depths (e.g., ∼20 cm in 2012L). This is perhaps not surprising, considering the point-measurement nature of the buoy observations of snow depth and the high variability of snow depth at small spatial scales. Considering the time mean per calendar week of all buoys (i.e., across all years) and the reconstructions, there is a reasonable degree of agreement between the two (Figure 7), and the root mean square error (RMSE) between the two time series is 3.8 cm. In early spring, at the same time as the OIB observations, the reconstruction tends to be slightly deeper than the mean buoy values by about 4 cm.

4.4. Sources of Uncertainty

4.4.1. Sublimation/Deposition

Reconstructing snow depth from snowfall alone neglects deposition on snow of frost and any mechanism by which snow is lost or redistributed. While limiting this study to the cold season (September through

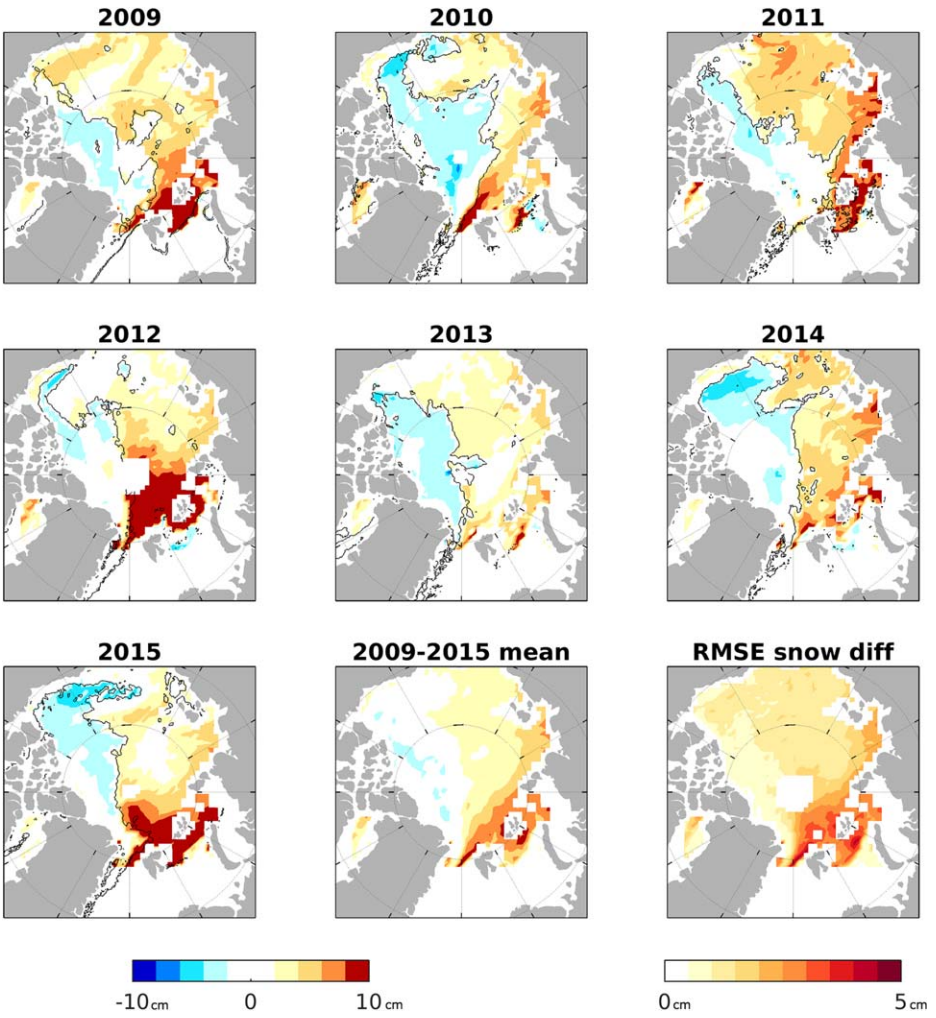

Figure 4. Difference in snow water equivalent between the reconstructed snow depth and the Warren weighted climatology. The black contour in individual years indicates the first-year/multiyear ice boundary.

April) mitigates snow loss due to melt, snow may still be lost through sublimation or by wind transport into leads, or gained through frost deposition. There is a large uncertainty in estimates of sublimation/deposition through the cold season in the Arctic (Liston & Sturm, 2004), and direct measurements are generally only available in the summer. Froyland et al. (2010) (and references within) provide estimates of June through September sublimation. For September, the only month in their analysis that has consistently negative temperatures (and serves as the closest analog to our cold season timeframe), they find a net deposition, though they point out that different estimates of sublimation/deposition for that month in the literature show a range of values that span both net sublimation or deposition. Nevertheless, ERA-Interim provides evaporation estimates that we use here to estimate the potential effects of sublimation on our analysis. Using equivalent notation as in equation (1), we calculated accumulated evaporation E as follows:

$$E(L,T)=\rho_T\sum_{t=1}^{T}e_{l,t}, \tag{2}$$

where $e_{l,t}$ is evaporation at time t and location l.

Figure 8 shows accumulated evaporation E and ice type. Accumulated winter evaporation values over MYI appears to be extremely low, generally less than 2 cm of SWE. Alternatively, winter evaporation over FYI appears at first to be significant, 4–10 cm of SWE and even higher values in the marginal ice zones, particularly in the Barents/Kara seas. However, we highlight two important considerations here. First, the

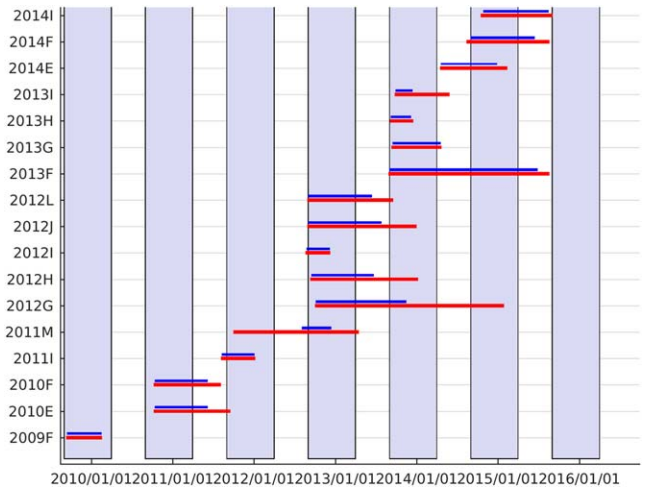

Figure 5. Lifetimes and nomenclature of the IMBs used in our analysis. The red lines indicate the lifetime of each buoy, the blue lines the period for which snow data were used in our study after quality control of the raw data. Blue shading indicates the cold season (1 September through 30 April).

evaporation output in ERA-Interim aggregates evaporation over open ocean and sea ice into a single value at each grid cell. Since evaporation over open ocean is much greater than over sea ice, aggregated evaporation is likely to be higher in the fall in regions of growing FYI, relatively low FYI concentration and high open water compared to regions of mainly MYI with little open water. Limiting our analysis to December-April when sea ice concentrations in regions of MYI and FYI are comparable (not shown) suggests that over this timeframe evaporation is extremely low (<2 cm of SWE) over most of the Arctic basin and over both FYI and MYI (Figure 8). Second, the sea-ice treatment in ERA-Interim is rudimentary: ice concentration is prescribed from observations, and the ice-covered part of a grid cell is assumed to be snow-free with constant 1.5 m thick sea ice. Thus, there is no distinction in the reanalysis model between relatively thin FYI and thick MYI, precluding the ERA-Interim atmosphere from correctly simulating different surface fluxes over these ice types.

4.4.2. Ice Divergence

Another source of uncertainty arises from sea ice divergence and new ice formation throughout the winter, whose effect is to reduce mean snow depth as the new ice has zero snow cover upon formation. Maksym and Markus (2008) investigated the role of this mechanism in Antarctica, and we apply their methodology here. Keeping the original notation in Maksym and Markus (2008), a new formulation for snow depth that accounts for ice divergence is derived as follows:

$$S_d(t) = S_{adv} + P\frac{(C-\Delta C)}{C} + P\frac{\Delta C}{2C}, \tag{3}$$

where $S_d(t)$ is snowdepth at time t, S_{adv} is advected snow depth, P is weekly snowfall at time t, C is sea ice concentration (SIC) at time t, and ΔC is the difference between SIC at time t and t – 1 after it has been

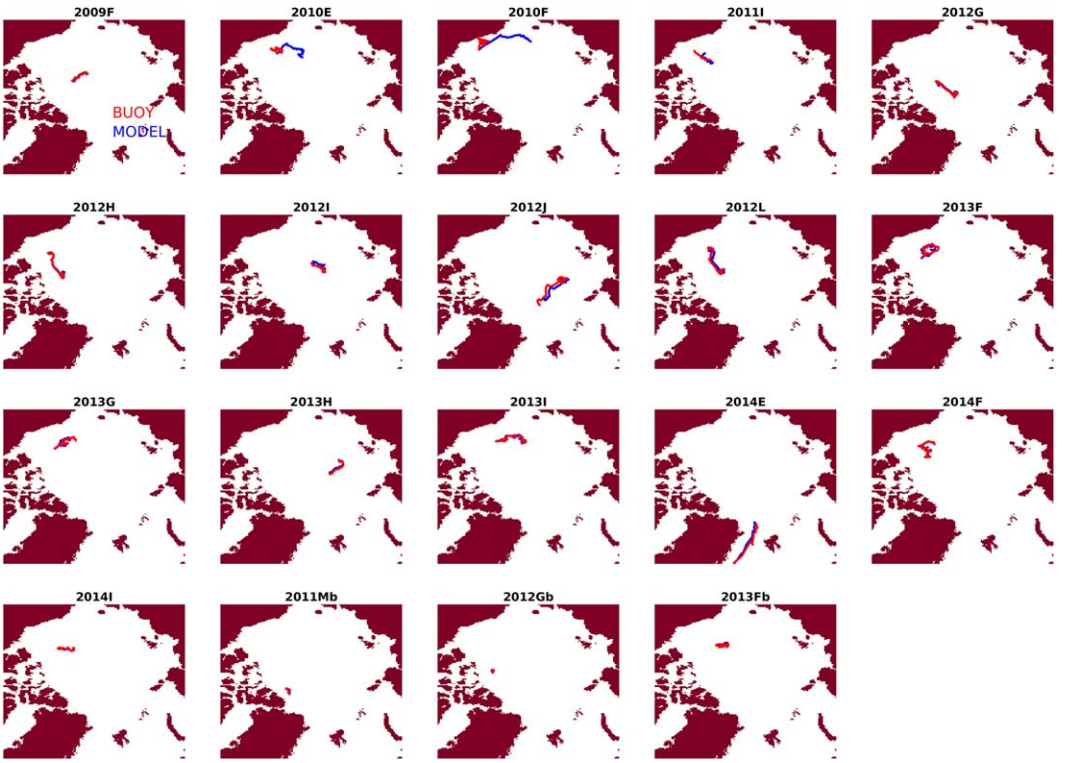

Figure 6. Buoy GPS tracks from the IMB buoys used in the study and modeled LITS tracks.

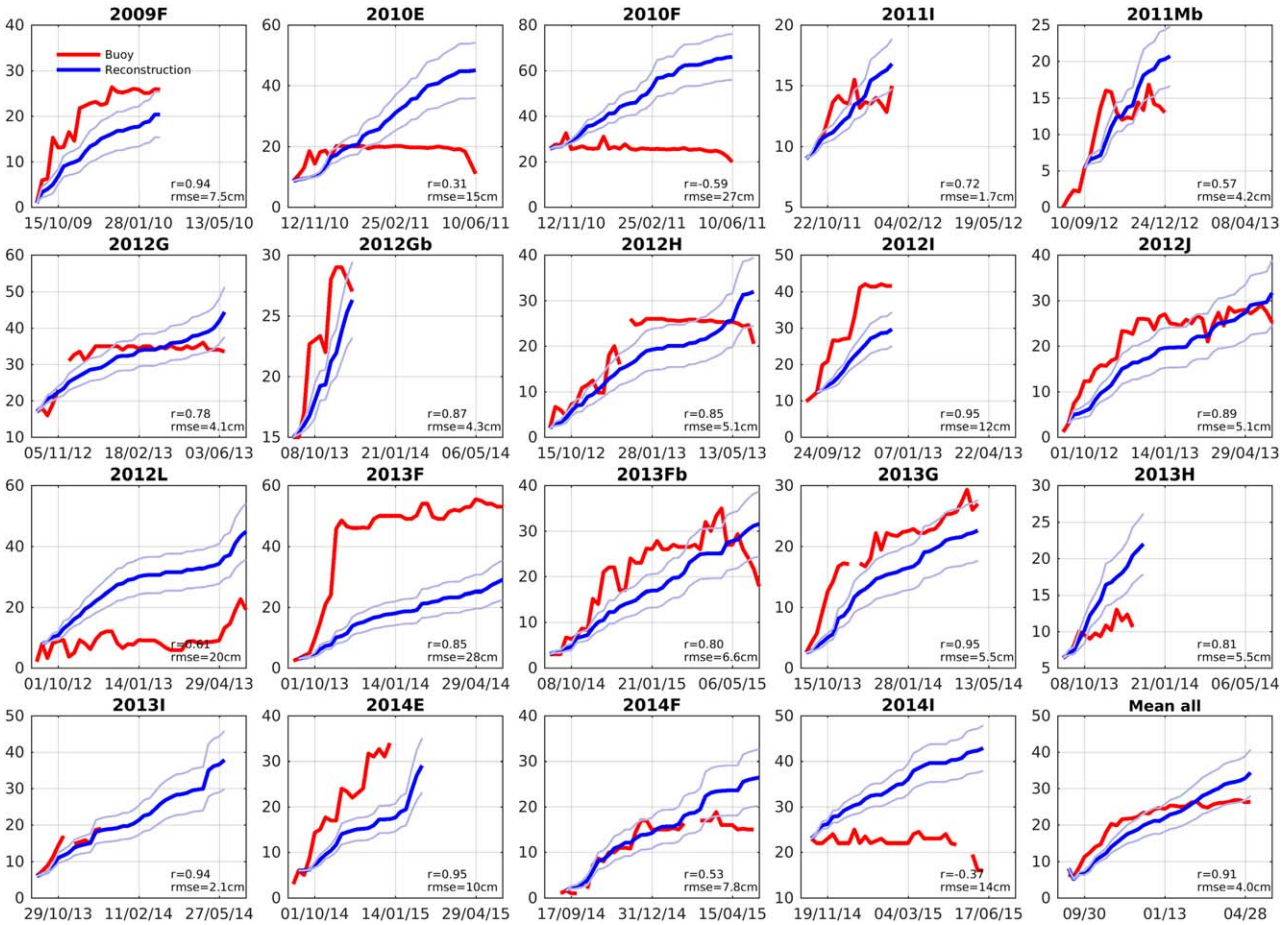

Figure 7. Weekly snowdepth in cm in IMB buoys (red) and reconstruction (blue). The mean values of the reconstruction using mean snow density is shown in bold blue, the range of the reconstruction using the upper and lower boundaries of snow density in Warren et al. (1999) are shown in thin blue lines. The bottom right plot shows the weekly-mean across all buoys and their reconstructions. The suffix 'b' after a buoy's plot title (e.g., "2012Gb") indicates the second winter of a multi-year buoy (see Figure 5 for buoy lifetimes). Date along x-asis is in DD/MM/YY format.

advected (i.e., $\Delta C = C(t) - C_{adv}(t-1 \Rightarrow t)$). ΔC provides an estimate of the fraction of new ice in a given pixel and is set to zero for converging conditions. The second term in 3 is divided by two because on average, the new ice will exist for only half the weekly timestep t, and so only receive half the snowfall on that week. Equation (3) can be reduced to

$$S_d(t) = S_{adv} + P\left(1 - \frac{\Delta C}{2C}\right), \tag{4}$$

and thus, for $\Delta C = 0$, we see that equation (4) is equivalent to equation (1) and $S_d = S$. Figure 9 shows mean reconstructed April S and S_d fields and the difference between the two. Over the OIB domain, differences are insignificant. Only along coastal areas in the East Siberian seas and Barents/Kara seas does divergence have a significant impact on reconstructed snow depth.

4.4.3. Choice of Reanalysis Data Product

How robust are our results to the choice of reanalysis for snowfall data? While ERA-Interim is one of the more accurate reanalysis products for precipitation in the Arctic (Lindsay et al., 2014), we have repeated the above calculations that use ERA-Interim with snowfall data taken from three other reanalysis: the Japanese Meteorological Agency's JRA-55 reanalysis (Kobayashi et al., 2015) and NASA's Modern-Era Retrospective Analysis for Research and Application version 1 (MERRA) and version 2 (MERRA2; Gelaro et al. 2017). We have also repeated the calculations with NASA's Global Precipitation Climatology Project (GPCP; Huffman & Bolvin 2013) precipitation data set, a global precipitation product produced by optimally merging estimates computed from microwave, infrared, and sounder data observed by satellites, and precipitation gauge

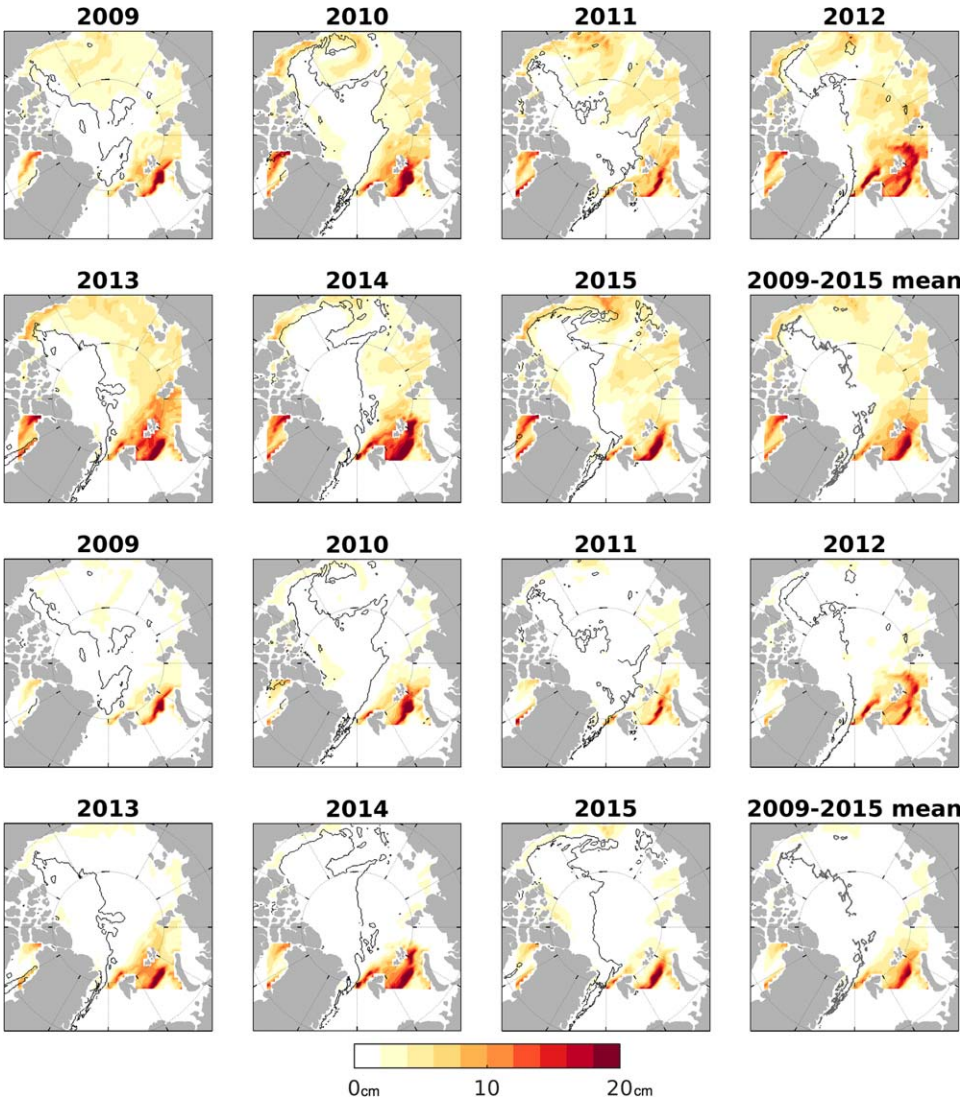

Figure 8. Accumulated evaporation (E) fields in SWE for late August-April (top two rows) and early December-April (bottom two rows). The black contours indicate the first-year/multiyear ice boundary.

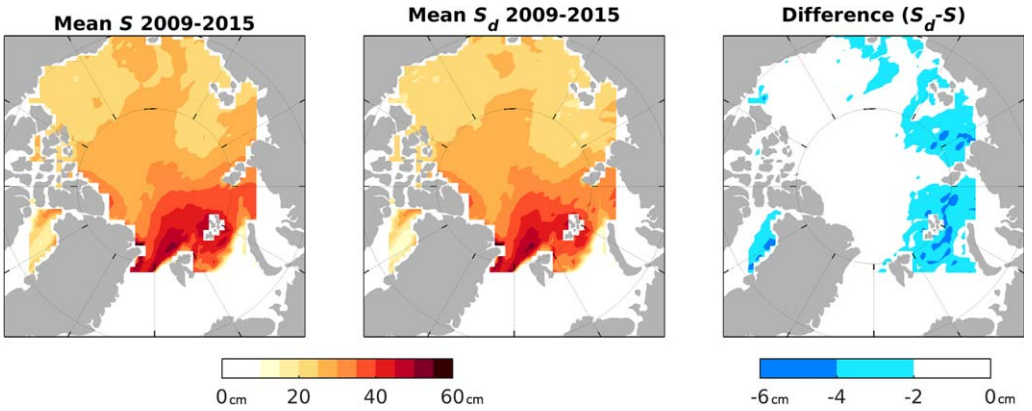

Figure 9. Mean 2009–2015 reconstructed spring snow depth (left) *S*), (middle) S_d (accounting for divergence), and (right) the difference (S_d-*S*).

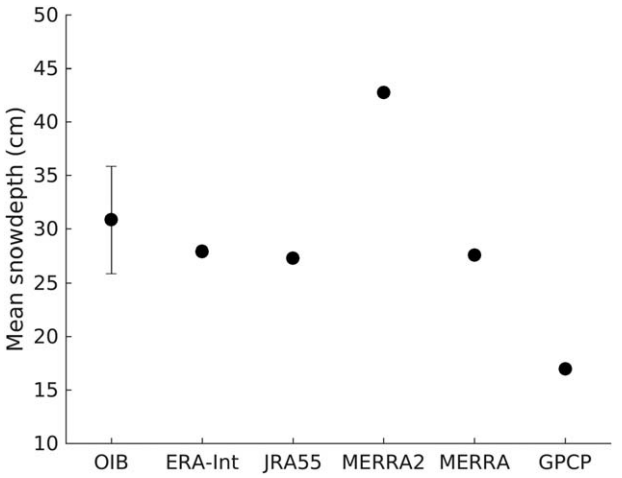

Figure 10. Mean snow depths for OIB and all reconstructions sampled along IceBridge flight tracks and dates.

analyses. Figure 10 shows the snowdepth reconstructions based on the different precipitation data sets compared with OIB snowdepths (i.e., the mean values for the 2009–2015 reconstructions sampled along OIB paths). Reconstructions using JRA-55 and MERRA are in close agreement to those using ERA-Interim and all three lie within the uncertainty boundaries of OIB, while the reconstruction using GPCP is too low and using MERRA-2 is too high. Figure 11 shows the equivalent of Figure 4i but using all reconstructions derived from the different precipitation products. It is noteworthy that despite the range in precipitation data sets, there is qualitative agreement in the spatial patterns of bias in the reconstructions compared to the weighted climatology.

4.5. Interannual Variability in Reconstruction 1980–2015

Since ERA-Interim reanalysis and the sea ice concentration and motion data sets extend back in time to 1979, we have extended the spring snow depth reconstruction back to 1980. We do this to place results from the OIB years of 2009–2015 in the context of the last few decades and to investigate the characteristics of interannual variability in snow depth. Figure 12a shows the time series of mean early April pan-Arctic snow depth for 1980–2015. For the whole period, the pan-Arctic mean value is 27.1 cm, almost identical to the pan-Arctic mean for 2009–2015 (27.0 cm). Overall, there is only a slight reduction in snow depth between 1980–1997 and 1998–2015 (28.3 cm versus 26.5 cm respectively), and a best-fit linear trend of ∼-0.6 cm per decade that is not significantly different to zero at a 95% significance level. Interannual variability spans a range of 22.5 cm to 33.3 cm and the standard deviation is 2.4 cm. Larger changes between the first and second halves the period are seen at the regional scale (Figure 12b), with losses of 5 cm or greater in the Chukchi, Kara and Barents seas, all regions that have undergone losses in both sea ice concentration and MYI fraction. Conversely, the reconstruction shows no major changes over large areas of the central basin.

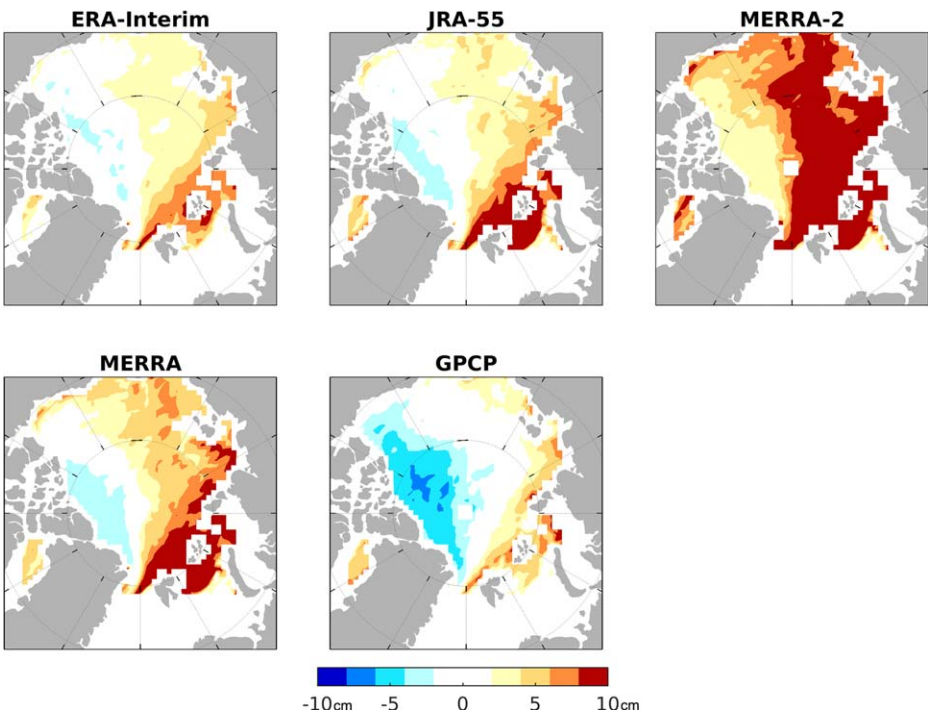

Figure 11. Mean differences over 2009–2015 in snow water equivalent in the reconstruction and the Warren weighted products.

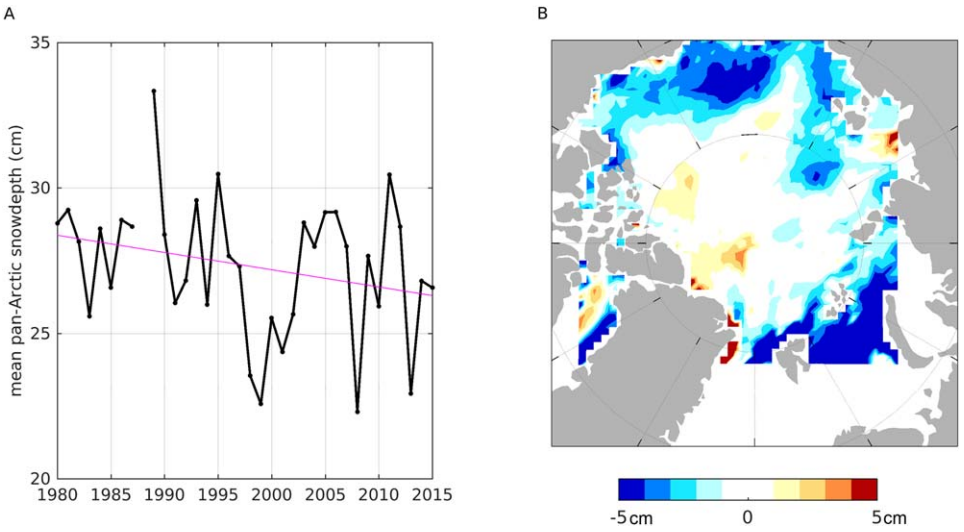

Figure 12. A) Mean pan-Arctic reconstructed snowdepth 1980–2015 (black line) and the best-fit linear trend (magenta), and B) difference in snow depth (in cm) between 1998–2015 and 1980–1997 in the reconstruction. We do not show data for 1988 as satellite sea ice concentration data do not exist for December 1987/January 1988.

5. Discussion and Conclusions

We have produced a reconstruction of Arctic snow using a Lagrangian ice-tracking algorithm, sea-ice motion and ERA-Interim reanalysis snowfall, and compared our results to observations of snow depth from NASA's OIB snow radar and CRREL's IMB buoys. The mean spring snow depth in the reconstruction is about 3 cm thinner than the mean OIB value, but about 4 cm deeper than the mean IMB values. These deviations are about 10–15% of the reconstructed mean. The shape of the reconstruction distributions also simulate well the OIB distributions, which the weighted climatology does not. At the local scale (10 km), the reconstruction provides an improvement over the weighted climatology for snow over FYI, but is biased thin for snow over MYI and is poor at capturing snow depth on individual buoys.

Discrepancies between the reconstruction and OIB and IMB values may result from snow loss mechanisms that are unaccounted for in our reconstruction, such as sublimation or snow loss to leads via wind transport, deposition of frost, and pre-existing summer snow over MYI. The magnitude and frequency of precipitation from any reanalysis contains uncertainty, which would lead to biases in ERA-Interim snowfall, even if it is currently the most reliable reanalysis for Arctic precipitation (Lindsay et al., 2014). Despite these caveats, our reconstruction raises important considerations.

The distinct snow depth distributions on FYI and MYI that have been found in the western Arctic in OIB data are not seen in the eastern Arctic in our reconstruction. Consequently, large biases exist in the eastern Arctic, particularly in the Atlantic sector, between our reconstruction and the weighted climatology that is used for the calculation of sea-ice thickness from satellite-derived observations of freeboard (Tilling et al., 2015), with 2–10 cm of SWE deeper snow in our reconstruction. Assuming hydrostatic equilibrium and using standard densities of snow and sea ice, a difference in snow depth of 10 cm of SWE equates to a retrieved thickness difference of 0.9 m for FYI or 0.71 m for MYI. These are significant differences that speak to the large impact of snow uncertainty on the uncertainty of sea-ice thickness estimates from satellite retrievals documented in Giles et al. (2007) and Tilling et al. (2015). We note that a field campaign found a deep March snow depth (49 $\pm$13 cm) north of Svalbard in 2015 (Merkouriadi et al., 2017), in good agreement with our reconstruction for that region. Conversely, our reconstruction in the western Arctic over MYI has a thinner snow depth than the weighted climatology, in agreement with previous results (Webster et al., 2014). If these patterns of snow depth bias in the weighted climatology are correct, this would result in satellite-derived estimates of sea ice thickness that use the weighted climatology being biased low over FYI in the eastern Arctic, but biased high over MYI in the western Arctic.

Extending our reconstruction to 1980 shows that reconstructed snow depths during the OIB period are typical of the last few decades, but can also fluctuate greatly between years. The impact that interannual

variability in snow depth has on derived sea-ice thickness from freeboard cannot be captured by the use of a snow depth climatology, which will lead to biases in the estimates of interannual variability in sea-ice thickness. It is important to note however that both the uncertainty in the OIB data (~6 cm, with a bias of ~2 cm) and the mean error in the reconstruction (~3 cm) are comparable or greater than the interannual variability in reconstructed mean snow depth (σ ~3 cm), and that, despite the agreement in snow depth distributions in Figure 2, the reconstruction does not capture particularly well the interannual variability in mean OIB snowdepths (Figure 2). Given the very small sample size (6 yearly means), we caution against over-interpreting the skill of the reconstruction in this regard. We note that interannual variability in mean snow depth obtained from other OIB algorithms is not consistent (see Figure 11 in Kwok et al., 2017).

For the period 1980–2015, our reconstruction shows a small decreasing trend in spring snow depth of 0.6 cm per decade, significantly smaller than the estimate of 2.9 cm per decade previously found in Webster et al. (2014) for the period 1950–2013, yet within the range of spring snow depth trends simulated by global climate models (GCMs) (Hezel et al., 2012). We note however that our reconstruction assumes all snow melts in the summer and cannot account for potential changes in the timing of snow depth accumulation on MYI – snow on MYI is likely to start accumulating later in late summer as the climate warms, resulting in lower spring snow depth even with no changes in cold season snowfall, a mechanism that has been shown to have an impact on MYI spring snow depths in GCMs (Blanchard-Wrigglesworth et al., 2015). We also do not account for rain on snow events, whose frequency and impact on the snow cover may have changed over the last few decades. Additionally, care must be taken when interpreting trends obtained from reanalysis products (Bengtsson et al., 2004).

Given the importance of snow on sea ice for Arctic climate, improved monitoring and knowledge of processes involving snow on sea ice would have a range of benefits for scientists and the growing body of stakeholders. With the upcoming launch of ICESat-2 and continuation of CryoSat-2, accurate estimates of Arctic snow depth are critical. Specifically extending coverage of snow observations in the eastern Arctic and continued monitoring on MYI in the western Arctic should be given high priority. We note that OIB extended flight surveys into the eastern Arctic north and east of Svalbard during the 2017 spring campaign. Continuing these efforts will aid in validating and improving the results shown in this paper.

Acknowledgments
We thank Bruno Tremblay, Charles Brunette and Bob Newton for sharing and helping with the LITS. We thank Stephen Warren for discussions on the topic of snow sublimation, and Richard Cullather and Angeline Pendergrass for providing help with retrieving reanalysis and GPCP data. We also thank two anonymous reviewers for their helpful comments and insights. E. Blanchard-Wrigglesworth, C. M. Bitz and S. Farrell were supported by NASA grant NNX14AI03G. M. Webster was funded by the National Aeronautics and Space Administration's Cryosphere Sciences Program. The IMB snow depth data for 2009–2015 are archived at: http://imb-crrel-dartmouth.org/imb.crrel/buoysum.htm. OIB Snow Radar L1B Geolocated Radar Echo Strength Profiles, Version 2, deconvolution and supporting information are archived at: http://nsidc.org/data/irsno1b. The wavelet processed snow depths are from the NOAA" WAV" Airborne Snow Radar - Snow Depth on Arctic Sea Ice Data Set, available at: ftp://ftp.star.nesdis.noaa.gov/pub/socd/lsa/SeaIceProducts/IceBridge/SnowDepth/. We provide a data set and documentation of our snow depth reconstruction at http://www.atmos.washington.edu/~ed/data/snow.

References

Bengtsson, L., Hagemann, S., & Hodges, K. I. (2004). Can climate trends be calculated from reanalysis data? *Journal of Geophysical Research*, *109*, D11111. https://doi.org/10.1029/2004JD004536

Blanchard-Wrigglesworth, E., Farrell, S., Newman, T., & Bitz, C. (2015). Snow cover on Arctic sea ice in observations and an Earth system model. *Geophysical Research Letters*, *42*, 10342–10348. https://doi.org/10.1002/2015GL066049

Breivik, L.-A., Eastwood, S., & Lavergne, T. (2012). Use of C-band scatterometer for sea ice edge identification. *IEEE Transactions on Geoscience and Remote Sensing*, *50*(7), 2669–2677.

Comiso, J. C., Parkinson, C. L., Gersten, R., & Stock, L. (2008). Accelerated decline in the Arctic sea ice cover. *Geophysical Research Letters*, *35*, L01703. https://doi.org/10.1029/2007GL031972

Dee, D. S., Uppala, A., Simmons, P., Berrisford, P., Poli, S., Kobayashi, U., et al. (2011). The ERA-Interim reanalysis: Configuration and performance of the data assimilation system. *Quarterly Journal of the Royal Meteorological Society*, *137*(656), 553–597.

DeRepentigny, P., Tremblay, L. B., Newton, R., & Pfirman, S. (2016). Patterns of sea ice retreat in the transition to a seasonally ice-free Arctic. *Journal of Climate*, *29*(19), 6993–7008.

Farrell, S. L., Kurtz, N., Connor, L. N., Elder, B. C., Leuschen, C., Markus, T., et al. (2012). A first assessment of IceBridge snow and ice thickness data over Arctic sea ice. *IEEE Transactions on Geoscience and Remote Sensing*, *50*(6), 2098–2111.

Froyland, H. K., Untersteiner, N., Town, M. S., & Warren, S. G. (2010). Evaporation from Arctic sea ice in summer during the International Geophysical Year, 1957–1958. *Journal of Geophysical Research: Atmospheres*, *115*, D15104. https://doi.org/10.1029/2009JD012769

Gelaro, R., McCarty, W., Suarez, M., Todling, R., Molod, A., Takacs, L., et al. (2017). The Modern-Era Retrospective Analysis for Research and Applications, version-2 (MERRA-2). *Journal of Climate*, *30*(14), 5419–5454. https://doi.org/10.1175/JCLI-D-16-0758.1

Giles, K., Laxon, S., Wingham, D., Wallis, D., Krabill, W., Leuschen, C., et al. (2007). Combined airborne laser and radar altimeter measurements over the Fram Strait in May 2002. *Remote Sensing of Environment*, *111*(2), 182–194.

Hezel, P., Zhang, X., Bitz, C., Kelly, B., & Massonnet, F. (2012). Projected decline in spring snow depth on Arctic sea ice caused by progressively later autumn open ocean freeze-up this century. *Geophysical Research Letters*, *39*, L17505. https://doi.org/10.1029/2012GL052794

Huffman, G. J., & Bolvin, D. T. (2013). Version 1.2 GPCP one-degree daily precipitation data set documentation, *GPCP*. Retrieved from ftp://rsd. gsfc. nasa. gov/pub/1dd-v1. 2/1DD_v1. 2_doc. pdf.].

Itkin, P., Spreen, G., Cheng, B., Doble, M., Girard-Ardhuin, F., Haapala, J., et al. (2017). Thin ice and storms: Sea ice deformation from buoy arrays deployed during N-ICE2015. *Journal of Geophysical Research: Oceans*, *122*, 4661–4674. https://doi.org/10.1002/2016JC012403

Kobayashi, S. O., Yukinari, Y., Harada, A., Ebita, M., Moriya, H., Onoda, K., et al. (2015). The JRA-55 reanalysis: General specifications and basic characteristics. *Journal of the Meteorological Society of Japan. Ser. II*, *93*(1), 5–48.

Koenig, L., Martin, S., Studinger, M., & Sonntag, J. (2010). Polar airborne observations fill gap in satellite data. *Eos, Transactions American Geophysical Union*, *91*(38), 333–334.

Kurtz, N., Markus, T., Farrell, S., Worthen, D., & Boisvert, L. (2011). Observations of recent Arctic sea ice volume loss and its impact on ocean-atmosphere energy exchange and ice production. *Journal of Geophysical Research*, *116*, C04015. https://doi.org/10.1029/2010JC006235

Kurtz, N. T., & Farrell, S. L. (2011). Large-scale surveys of snow depth on Arctic sea ice from Operation IceBridge. *Geophysical Research Letters*, *38*, L20505. https://doi.org/10.1029/2011GL049216

Kwok, R., & Cunningham, G. (2008). ICESat over Arctic sea ice: Estimation of snow depth and ice thickness. *Journal of Geophysical Research*, *113*, C08010. https://doi.org/10.1029/2008JC004753

Kwok, R., & Cunningham, G. (2015). Variability of Arctic sea ice thickness and volume from cryosat-2. *Philosophical Transactions of the Royal Society A: Mathematical, Physical and Engineering Sciences*, *373*(2045), 20140,157.

Kwok, R., Kurtz, N., Brucker, T., Ivanoff, L., Newman, A. T., Farrell, S., et al. (2017). Inter-comparison of snow depth retrievals over Arctic sea ice from radar data acquired by Operation IceBridge. *The Cryosphere Discussions*, *11*(6), 2571.

Kwok, R., & Rothrock, D. (2009). Decline in Arctic sea ice thickness from submarine and ICESat records: 1958–2008. *Geophysical Research Letters*, *36*, L15501. https://doi.org/10.1029/2009GL039035

Laxon, S., Peacock, N., & Smith, D. (2003). High interannual variability of sea ice thickness in the Arctic region. *Nature*, *425*(6961), 947–950.

Laxon, S. W., Giles, K. A., Ridout, A. L., Wingham, D. J., Willatt, R., Cullen, R. et al. (2013). CryoSat-2 estimates of Arctic sea ice thickness and volume. *Geophysical Research Letters*, *40*, 732–737. https://doi.org/10.1002/grl.50193

Leuschen, C. (2010, updated 2017), *IceBridge snow radar L1B geolocated radar echo strength profiles*. Boulder, CO: NASA DAAC at the National Snow and Ice Data Center. https://doi.org/10.5067/FAZTWP500V70

Lindsay, R. (1998). Temporal variability of the energy balance of thick Arctic pack ice. *Journal of Climate*, *11*(3), 313–333.

Lindsay, R., Wensnahan, M., Schweiger, A., & Zhang, J. (2014). Evaluation of seven different atmospheric reanalysis products in the Arctic. *Journal of Climate*, *27*(7), 2588–2606.

Liston, G., & Sturm, M. (2004). The role of winter sublimation in the Arctic moisture budget. *Hydrology Research*, *35*(4–5), 325–334.

Maksym, T., & Markus, T. (2008). Antarctic sea ice thickness and snow-to-ice conversion from atmospheric reanalysis and passive microwave snow depth. *Journal of Geophysical Research: Oceans*, *113*, C02S12. https://doi.org/10.1029/2006JC004085

Maslanik, J., Stroeve, J., Fowler, C., & Emery, W. (2011). Distribution and trends in Arctic sea ice age through spring 2011. *Geophysical Research Letters*, *38*, L13502. https://doi.org/10.1029/2011GL047735

Maykut, G. A., & Untersteiner, N. (1971). Some results from a time-dependent thermodynamic model of sea ice. *Journal of Geophysical Research*, *76*(6), 1550–1575.

Meier, W., Fetterer, F., Savoie, M., Mallory, S., Duerr, R., & Stroeve, J. (2013, updated 2015). *NOAA/NSIDC climate data record of passive microwave sea ice concentration, version 2*. Boulder, CO: National Snow and Ice Data Center.

Merkouriadi, I., Gallet, J.-C., Liston, G. E., Polashenski, C., Graham, R. M., Rösel, A., & Gerland, S. (2017). Winter snow conditions on Arctic sea ice north of Svalbard during the Norwegian young sea ICE (N-ICE2015) expedition. *Journal of Geophysical Research: Atmospheres*, *122*, 10837–10854. https://doi.org/10.1002/2017JD026753

Newman, T., Farrell, S., Richter-Menge, L. J., Connor, L. N., Kurtz, N. T., Elder, B. C., & McAdoo, D. (2014). Assessment of radar-derived snow depth over Arctic sea ice. *Journal of Geophysical Research: Oceans*, *119*, 8578–8602. https://doi.org/10.1002/2014JC010284

Perovich, D., Grenfell, T., Light, B., & Hobbs, P. (2002). Seasonal evolution of the albedo of multiyear Arctic sea ice. *Journal of Geophysical Research*, *107*(C10), 8044. https://doi.org/10.1029/2000JC000438

Perovich, D., Richter-Menge, Elder, J., Arbetter, B., Claffey, T. K., & Polashenski, C. (2017). Observing and understanding climate change: Monitoring the mass balance, motion, and thickness of Arctic sea ice. Retrieved from http://IMB.crrel.usace.army.mil

Petrich, C., Eicken, H., Polashenski, C. M., Sturm, M., Harbeck, J. P., Perovich, D. K., & Finnegan, D. C. (2012). Snow dunes: A controlling factor of melt pond distribution on Arctic sea ice. *Journal of Geophysical Research*, *117*, C09029. https://doi.org/10.1029/2012JC008192

Richter-Menge, J. A., Perovich, D. K., Elder, B. C., Claffey, K., Rigor, I., & Ortmeyer, M. (2006). Ice mass-balance buoys: A tool for measuring and attributing changes in the thickness of the Arctic sea-ice cover. *Annals of Glaciology*, *44*(1), 205–210.

Ricker, R., Hendricks, S., Helm, V., Skourup, H., & Davidson, M. (2014). Sensitivity of CryoSat-2 Arctic sea-ice freeboard and thickness on radar-waveform interpretation. *The Cryosphere*, *8*(4), 1607–1622.

Serreze, M. C., Barrett, A. P., & Lo, F. (2005). Northern high-latitude precipitation as depicted by atmospheric reanalyses and satellite retrievals. *Monthly Weather Review*, *133*(12), 3407–3430.

Sturm, M., Holmgren, J., & Perovich, D. K. (2002b). Winter snow cover on the sea ice of the Arctic Ocean at the Surface Heat Budget of the Arctic Ocean (SHEBA): Temporal evolution and spatial variability. *Journal of Geophysical Research*, *107*(C10), 8047. https://doi.org/10.1029/2000JC000400

Sturm, M., Perovich, D. K., & Holmgren, J. (2002a). Thermal conductivity and heat transfer through the snow on the ice of the beaufort sea. *Journal of Geophysical Research*, *107*(C10), 8043. https://doi.org/10.1029/2000JC000409

Tilling, R. L., Ridout, A., Shepherd, A., & Wingham, D. J. (2015). Increased Arctic sea ice volume after anomalously low melting in 2013. *Nature Geoscience*, *8*(8), 643–646.

Tschudi, M., Fowler, C., Maslanik, J., Stewart, J., & Meier, W. (2016). *Polar Pathfinder daily 25km EASE-grid sea ice motion vectors, version 3*. Boulder, CO: National Snow and Ice Data Center Distributed Active Archive Center. https://doi.org/10.5067/O57VAIT2AYYY

Warren, S. G., Rigor, I. G., Untersteiner, N., Radionov, V. F., Bryazgin, N. N., Aleksandrov, Y. I., & Colony, R. (1999). Snow depth on Arctic sea ice. *Journal of Climate*, *12*(6), 1814–1829.

Webster, M. A., Rigor, I. G., Nghiem, S. V., Kurtz, N. T., Farrell, S. L., Perovich, D. K., & Sturm, M. (2014). Interdecadal changes in snow depth on Arctic sea ice. *Journal of Geophysical Research: Oceans*, *119*, 5395–5406. https://doi.org/10.1002/2014JC009985

Webster, M. A., Rigor, I. G., Perovich, D. K., Richter-Menge, J. A., Polashenski, C. M., & Light, B. (2015). Seasonal evolution of melt ponds on Arctic sea ice. *Journal of Geophysical Research: Oceans*, *120*, 5968–5982. https://doi.org/10.1002/2015JC011030

Yan, J.-B., Alvestegui, D. G.-G., McDaniel, J. W., Li, Y., Gogineni, S., Rodriguez-Morales, F., et al. (2017). Ultrawideband FMCW radar for airborne measurements of snow over sea ice and land. *IEEE Transactions on Geoscience and Remote Sensing*, *55*(2), 834–843.